29th EPS Conference on Plasma Phys. and Contr. Fusion Montreux, 17-21 June 2002 ECA Vol. **26B**, P-1.110 (2002)

Tokamak Edge E_r and Transport Studies by Turbulence and Divertor Codes

Y. Nishimura, D. Coster, B. Scott

Max-Planck-Institut für Plasmaphysik, EURATOM Association, D-85748 Garching, Germany

In divertor transport simulations, perpendicular transport is given empirically and usually assumed to be constant in time and space. In reality, anomalous $D_\perp$ and $\chi_\perp$ are known to be sensitive functions of the gradients [1] (the density gradient ∇n and the temperature gradient ∇T) and various parameters

$$D = D\left(\mathbf{r}, t\right) = D\left(\nabla n, \nabla T_e, \nabla T_i, \nu, \omega_E, ...Z_{eff}, ...P_{aux}, ...\right). \quad (1)$$

For the purpose of computing transport phenomena correctly, we need to employ first principle (theory) based transport coefficients. In this work, numerical coupling of perpendicular transport between a turbulence code DALF [2] and a divertor code B2 [3] is pursued. We also model H-modes [4] incorporating self-consistent E_r as well as $E \times B$ shear stabilisation of turbulence [5] .

The following transport coefficients are imported from DALF to B2 based on Fick's law and Fourier's law. In MKS units this reads $D = - < \bar{n}\bar{v_x} > (n/\nabla n) \times C_s\rho_s^2/L_\perp^2$, $\chi = - < 3/2\bar{n}\bar{T} > (T/\nabla T) \times C_s\rho_s^2/L_\perp^2$, where ρ_s is square root the mass ratio times the ion Larmor radius, C_s is the sound velocity and ∇n and ∇T are that of the equilibrium. The flux $< \bar{n}\bar{v_x} >$ in a dimensionless form is calculated from DALF, where the factor $C_s\rho_s^2/L_\perp^2$ is computed as an internal parameter in B2. We employed a two dimensional sheared slab model for the turbulence computation. In addition to the Hasegawa-Wakatani model [1] , T_e and T_i equations are evolved in an electrostatic limit [2] . In practice we prepare a fitted numerical database beforehand for D and χ 's. The largest advantage is numerical stability for the implicit solver of B2. Alternatively running DALF and B2 (direct coupling) is employed rather to pre-condition and to narrow down the parameter space. Up to seven different parameters are practically approachable in the current computational settings.

Fitting is done to the time averaged outputs from DALF by Chebyshev polynomials [6] . Transport as function of plasma parameters are expanded in the form

$$D\left(\mathbf{r}, t\right) = \sum A\left(i_n, i_t, i_i, i_\nu, i_\omega...\right) T_{i_n}(w_n) \times T_{i_t}(w_t) \times T_{i_i}(w_i) \times T_{i_\nu}(\nu) \times T_{i_\omega}(\omega_E)... \quad (2)$$

where $w_n, w_t,$ and w_i are the indices of $\nabla n, \nabla T_e,$ and ∇T_i . Here, ν and ω_E represent electron collisionality and the $E \times B$ shear parameter [5] respectively. An example of two dimensional fitting is shown in Ref. 7).

An example of divertor simulation with constant core heat flux is shown aiming at reconstructing the H-mode. Transport coefficients are space and time dependent as signified in Eq.(2). If the temperature at the core is fixed, the heat flux adjusts itself to relax the radial profile and will not make significant difference with the constant D and χ cases. The reference configuration is from an ASDEX Upgrade single null divertor shot. A grid size of 96×36 is used to resolve the structure of the radial electric field in

the vicinity of the divertor separatrix (the radial grids are packed near the separatrix). Dirichlet boundary conditions are taken for n at the core ($6 \times 10^{19} m^{-3}$). Neumann boundary conditions for T_e and T_i at the core correspond to a total heating power of $3.7MW$. The rest of the parameters are the same as in Ref. 7). Essentially the radial transport in the closed field line regions can be understood as a one dimensional problem. Responding to the dynamics of drift-wave turbulence [1] (steeper the gradients, larger the transport) the plasma is transported to the turbulent side and make the profile rather uniform compared to the constant constant D and χ cases. Turbulence makes the plasma profile stiff. This feature is captured in the region $y \leq 0(m)$. The increase of transport coefficients toward the edge in Fig.1(b) (large dissipation at the low temperature regions) is the response to the ν dependence of Eq.(2).

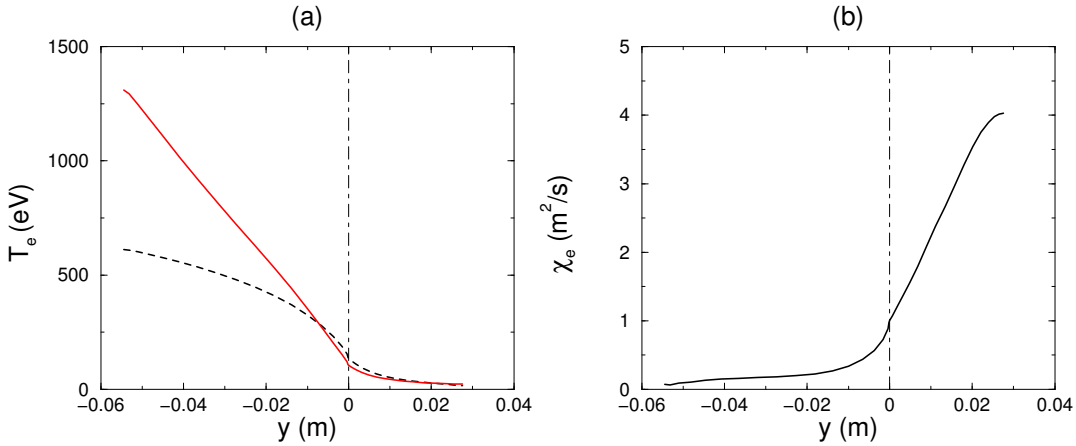

Figure 1: (a) Radial electron temperature profile from B2 simulation at the outboard midplane. Black dashed line: In the absence of turbulence effects [$D = 0.5(m^2/s)$ and $\chi = 0.7(m^2/s)$ constant in time and space]. Red line: as a response of drift-wave turbulence. The separatrix is signified by dashed lines at $y = 0(m)$. (b) Radial profile of converged $\chi_e(m^2/s)$ values.

The Braginskii transport model of the B2 code incorporates guiding-centre plasma drifts self-consistently [8] and generates E_r shear in the presence of steep gradients. Here we briefly review the generation mechanism of electric field both inside and outside the separatrix. Inside the divertor separatrix, the electric field is described by the radial ion momentum balance of the Braginskii set of equations [9] . The original Braginskii equations (for one component ion) solve ten equations, that are mass, momentum, and energy balance equations, for ten unknowns $n_i, n_e, \mathbf{V}_i, \mathbf{V}_e, T_i$, and T_e . The ion momentum balance equation is given by

$$m_i n_i \left[\frac{\partial}{\partial t} (\mathbf{V}) + (\mathbf{V} \cdot \nabla) \mathbf{V} \right] = -\nabla p_i - \nabla \cdot \Pi_i + e n_i (-\nabla \phi + \mathbf{V} \times \mathbf{B}) + \mathbf{R} + \mathbf{S^m}. \quad (3)$$

The terms on the right hand are the pressure gradient, stress tensor, Lorentz force and the collision terms. In a steady state $\partial_t \rightarrow 0$, when the flow term $\mathbf{V} \times \mathbf{B}$ are less dominant [10] , the radial component gives an approximate relation $\phi \sim -p_i$. Within the B2 formulation, the equations are reduced to five, solving for $n (= n_i = n_e)$, $V_{\|}$, T_i ,

T_e , and the electrostatic potential ϕ . The perpendicular dynamics are given by the guiding centre approximation. The balance between diamagnetic and the $E \times B$ drifts in the quasi-neutral relation determines the electrostatic potential.

On the other hand, the electric field in the scrape off layer (SOL) is determined by Bohm sheath dynamics. The ions enter the sheath regions (the divertor plates) at the sound speed: $J_i = n_0 e C_s$. On the other hand, the electrons follow the Boltzmann relation closely: $J_e = -(n_0 e C_s/4) \exp(e\phi/T_e)$. The electrostatic potential is determined by $J_i + J_e = 0$ toward the divertor plate. We obtain an approximate relation $\phi \sim T_e$.

Figure 2(a) shows the radial profile of the electrostatic potential obtained from a B2 simulation. As predicted by the theory, profiles follow $\phi \sim -p_i$ inside the separatrix and $\phi \sim T_e$ in SOL. The anomalous perpendicular dynamics and corresponding dissipation mechanism (which connects the solution inside and outside the divertor separatrix) determine the scale length of the boundary layer. Figure 2(b) shows the radial electrostatic field E_r , which is simply a radial derivative of Fig. 2(a).

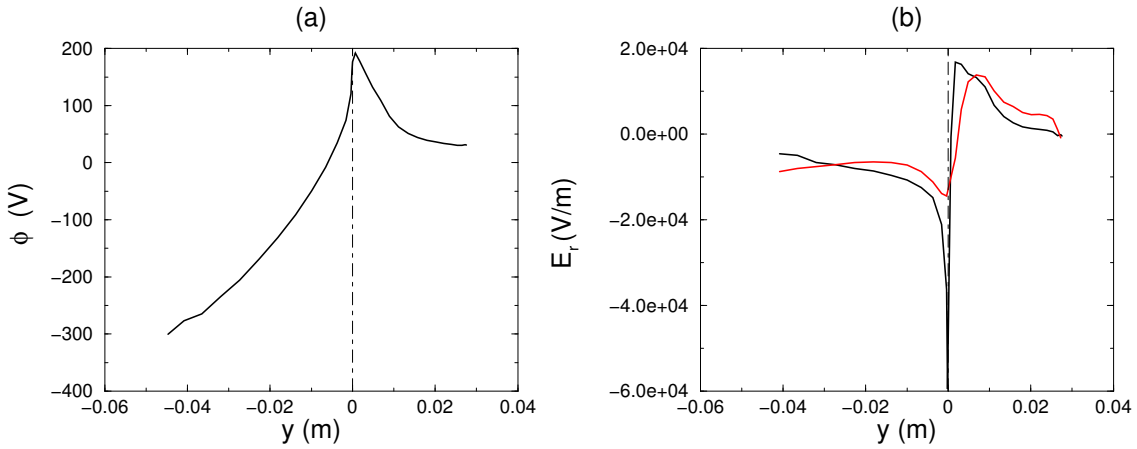

Figure 2: (a) Radial profile of electrostatic potential on the outboard midplane, and (b) radial electric field (both from B2 simulation in the absence of turbulence effects when D and χ 's constant in time and space. Red line : radial electric field as a response of turbulence.

Now, let us discuss the relation of our coupled simulation model to the L to H transition [4] . Note the extremely short scale length of dE_r/dy [the black solid line in Fig.2(b)]. The steepness near the separatrix is caused by perpendicular transport with constant D and χ 's. [At the separatrix the absolute value of the E_r shear is an order (or two) of magnitude larger than the experiments]. As in the red solid line of Fig.2(b), turbulence modification to the Braginskii electric field smoothes out the localised structure.

The Braginskii type external electric field can enter the turbulence model as a background $E \times B$ shear parameter [ω_E of Eq.(2)]. Simulation results from the turbulence model suggest a monotonic decrease of the radial transport as the value ω_E increase. Figure 3(a) is a fitted DALF output of the diffusion coefficient as a function of ω_E and the gradients $w_n = w_t = w_i$ [Note that the turbulence model includes Reynolds stress, and thus the electric fields are the combination of the Braginskii type and zonal flows [11]].

There are two transport mechanisms in Figure 3(a) that were already described above; transport increases with the gradients (drift-wave dynamics) and transport decreases with the external $E \times B$ shear flow [5]. If the density and temperature steepen in the edge regions [by an external source [12], for example] and reach a critical gradient, shear flow stabilisation becomes dominant and the transport level can go down the hill of the curved surface [follow the solid curve in Fig.3(a)]. Interestingly, the solid line is still monotonically increasing along the gradient axis. Projection of the solid line to the two dimensional plane will give the well-known L to H transition curve [see Fig.3(b)].

In this work, we have presented divertor simulation employing space and time dependent transport coefficients. Our preliminary results related to L-H transition are given.

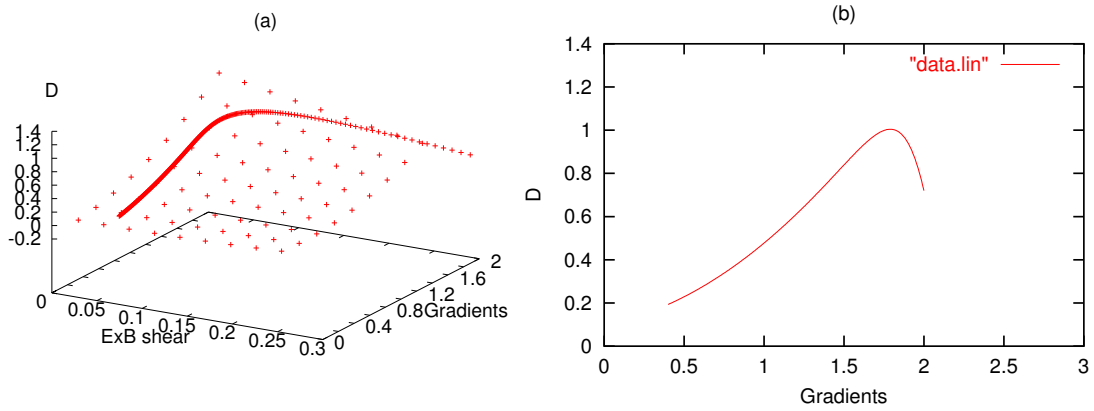

Figure 3: (a) Fitted DALF output of diffusion coefficient as a function of external ω_E and the gradients $w_n = w_t = w_i$. The surface is tilted. The value D increase in the direction of the gradients and decrease in the direction of $E \times B$ shear. (b) A projection of L to H transition curve of (a).

References

1) M.Wakatani and A.Hasegawa, Phys. Fluids **27**, 611 (1984).
2) B.D.Scott, Phys. Fluids B **4**, 2468 (1992).
3) B.J.Braams, Next European Torus Technical Report 68 (1987).
4) F.Wagner *et al.*, Phys. Rev. Lett. **49**, 1408 (1982).
5) H.Biglari, P.H.Diamomd, and P.W.Terry, Phys. Fluids B **2**, 1 (1990).
6) Cheney and Kincaid, *Numerical Mathematics and Computing*, 3rd Edition Brooks/Cole Publishing Company, p.389.
7) Y.Nishimura, D.Coster, J.Kim, and B.Scott, Contrib. Plasma Phys. **42**, 379 (2002).
8) V.A.Rozhansky, S.P.Voskoboynikov, E.G.Kaveeva, D.P.Coster, and R.Schneider, Nucl. Fusion **41**, 387 (2001).
9) S.I.Braginskii, In Reviews of Plasma Physics, Vol. 1 (ed. M.A.Leontovich), Consultants Bureau, New York, 205-311 (1965).
10) For thorough comparison of the terms, see T.D.Rognlien, D.D.Ryutov, N.Mattor, and G.D.Porter, Phys. Plasmas **6**, 1851 (1999).
11) A.Hasegawa and M.Wakatani, Phys. Rev. Lett. **59**, 1581 (1987).
12) Y.Hamada *et al.*, in Proceedings of the 17th IAEA Fusion Energy Conference (IAEA-F1-CN-69/PD , 1998) reveals heat pulse induced L-H transitions after sawtooth events.